ELSEVIER

Surface Science 329 (1995) 255–268

surface science

Predicting STM images of molecular adsorbates

V.M. Hallmark, S. Chiang *,1

IBM Research Division, Almaden Research Center, San Jose, CA 95120, USA

Received 2 June 1994; accepted for publication 18 January 1995

Abstract

Extended Hückel theory forms the basis of a simple computational method for predicting scanning tunneling microscopy images for molecules adsorbed onto metal surfaces. Development of the technique is described, including adsorbate geometry selection, calculation of electronic structure images, and comparison of the modeled images with both experiment and isolated molecule calculations. This technique is shown to reproduce such experimentally observed image features as detailed internal structure and resolution and bias effects. Systems considered include naphthalene, azulene, and a range of methylazulenes on Pt(111), benzene and CO on Rh(111), graphite, and fluorobenzene on Pt(111).

Keywords: Aromatics; Chemisorption; Electro density calculations; Platinum; Scanning tunneling microscopy; Semi-empirical models and model calculations; Solid–gas interfaces

1. Introduction

Simple molecular orbital theory has been used previously for comparison with scanning tunneling microscopy (STM) images of adsorbed molecules. For example, in the case of copper phthalocyanine adsorbed on Cu(100), the lowest unoccupied and highest occupied molecular orbitals (LUMO and HOMO, respectively) calculated by extended Hückel theory displayed close agreement with the experimentally observed unoccupied and occupied states' STM images [1]. HOMO and LUMO plots calculated by ab initio Hartree–Fock methods were also in accord with experiment in the case of alkylcyanobiphenyl liquid-crystals on graphite substrates [2]. These results clearly demonstrated that STM probes the electronic structure of the sample, rather than actual atomic topography. It is somewhat surprising, however, that the electronic states calculated for the *isolated* molecule were adequate for predicting the electronic structure of the *adsorbed* molecule. Indeed, in the case of naphthalene, its isomer azulene, and a number of substituted azulenes adsorbed on Pt(111), molecular orbital calculations for the isolated molecule do not reproduce well the details of the STM images [3]. For these systems, good agreement between experiment and calculation is only obtained after explicit inclusion of the metal substrate via a modified computational methodology. This paper describes in detail this procedure for calculating unoccupied and occupied state electronic structure for adsorbed molecules, the origin of the improved agreement, comparison with previously published experimental data, and extension of the technique to other systems.

---

* Corresponding author. Fax: +1 916 7524717; E-mail: chiang@physics.ucdavis.edu.

[1] Present address: Department of Physics, University of California, Davis, CA 95616, USA.

SSDI 0039-6028(95)00047-X

2. Background

In the early STM theory of Tersoff and Hamann [4] the tunneling current, I, at the position of the tip, r_0, in the limits of small voltage and temperature and arbitrarily localized tip wavefunctions, is proportional to the surface local density of states (LDOS) at the Fermi level, E_F,

$$I \propto \sum_{\nu} |\Psi(r_0)|^2 \delta(E_\nu - E_F). \tag{1}$$

This observation provides the basis for the early calculations of HOMO and LUMO states for comparison with STM data, since these states are those nearest to the Fermi level for the case of isolated molecules. Evaluation of the sample wavefunctions, Ψ, in the case of molecules, is easily accomplished by means of extended Hückel theory (EHT) [5]. This linear combination of atomic orbitals (LCAO) method departs from self-consistent field (SCF) methods in that integrals are evaluated empirically by use of experimental information such as atomic ionization potentials and electron affinities, and no iteration is performed. The spatial dependence of a molecular orbital, e.g. at a constant height above the molecular system, may be plotted by calculating the appropriate linear combination of atomic orbitals as a function of position.

To extend this simple approach to adsorbed rather than isolated molecules, EHT calculations may be performed for systems consisting of molecules plus metal clusters with the appropriate surface structure. For molecular adsorption onto metal surfaces, a number of calculational parameters must be determined. The choice of cluster size, both lateral extent and number of layers, may affect the results. Of critical importance are the binding site, molecular orientation with respect to the substrate lattice and molecule–metal separation. These issues have been previously addressed for naphthalene and azulene adsorption on Pt(111) via extended Hückel calculations [6]. In that approach, binding energy curves, such as those shown for naphthalene on Pt(111) in Fig. 1, were utilized to make predictions about the low energy adsorption geometry. Binding energies were calculated as a function of molecule–metal separation for naphthalene adsorbed in three low symmetry adsorption sites on a Pt_{13} or Pt_{14} cluster, with various orientations of the long molecular axis with respect to the metal lattice directions (see Fig. 2). Comparison of *relative* binding energies for the various adsorption sites and orientations is expected to be more reliable than the absolute values of individual binding energies. Such a comparison suggests that the (slightly) energetically preferred adsorption site is with the bridge-bond of the naphthalene molecule located on-top of a platinum atom, with the long axis of the molecule aligned along the near-neighbor direction of the substrate lattice. However, the low energy differences between two orientations in the on-top position suggests that rotation of the naphthalene within this site is likely to be facile. The similarity of these energies to that for the 2-fold site with 90° orientation also indicates that translational motion may be possible by some pathway of connecting low-energy adsorption geometries. Of course, the barrier heights for transition states with geometries separating these local minima adsorption sites are central to determining translational diffusion and rotational reorientation rates as a function of temperature. Such barrier heights can be estimated by calculating energies for molecular adsorption geometries along a selected path between the high symmetry adsorption sites, and in these cases appear to be on the order of a few tenths of an eV for rotational reorientation. However, as mentioned previously, while extended Hückel theory gives good trends for chemisorption energies, quantitative values are typically inaccurate [7].

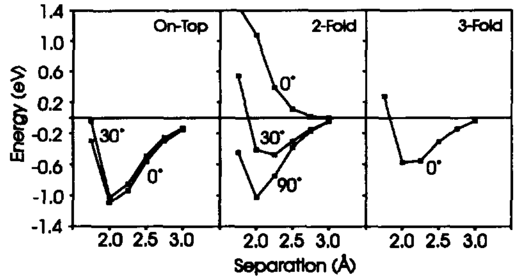

Fig. 1. Binding energy curves for naphthalene adsorbed on Pt_{13} and Pt_{14} (111) clusters. Three different binding sites were investigated: on-top (6-fold symmetric), 2-fold (bridge) and 3-fold (hollow). The effect of rotation of the long molecular axis with respect to the close-packed direction of the Pt substrate was also explored. See Fig. 2 for schematic diagrams of the adsorption geometries.

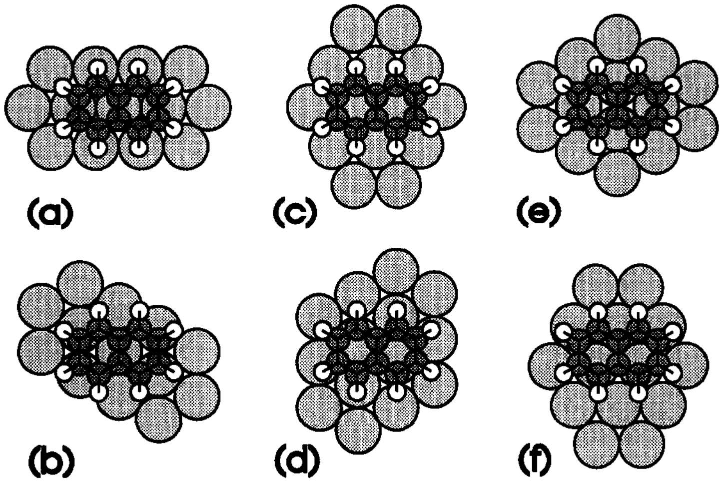

Fig. 2. Schematic diagrams of the adsorption geometries for naphthalene on Pt clusters used in the calculations of Fig. 1. One layer thick Pt clusters are used. On-top adsorption sites: (a) 0°, (b) 30°. Two-fold sites: (c) 0°, (d) 30°, (e) 90°. Three-fold site: (f) 0°.

These three theoretical observations have been verified by STM experiment – naphthalene has been assigned to the on-top, 0° adsorption site, naphthalene is observed to undergo rotational reorientation at room temperature when not confined within close-packed domains, and translation of naphthalene is discernible but less prevalent than rotation [8].

The surprisingly good agreement between experiment and predictions from such simple energetic calculations suggests that EHT methods are potentially appropriate models of these molecular adsorbate systems. Thus, utilization of this computational method as the basis of calculations of LDOS plots for comparison with STM images is plausible. It will be shown that, in fact, such a methodology provides extremely good agreement with experimental results for naphthalene and a number of substituted azulenes, and also for a number of other systems studied previously by STM. Results from such calculations can not only qualitatively predict the overall molecular structure as measured by STM, but comparison of experiment and theory can also be used to gain more detailed insight about the electronic structures of the adsorbate and to assign the origin of internal molecular features in STM images.

3. Theoretical methods

Extended Hückel calculations were performed via the program FORTICON 8, supplied by Quantum Chemistry Program Exchange (QCPE). Hückel parameters for the platinum clusters, taken from the literature [9], are given in Table 1. For each molecule investigated, binding energy curves analogous to those shown in Fig. 1 were computed. The low energy site and orientation assignment was then utilized for further calculations. No other energy minimization, such as relaxation of the molecular structure, was executed.

For the selected adsorption position, electronic structures were computed by selecting an imaging plane at a constant height above the metal surface, and then directly calculating the sum of the magnitudes of all molecular orbitals at each point within the plane. Typically, electronic structure maps were 100 points × 100 points in size with corresponding spatial extent of 15 Å × 15 Å. The results of this procedure correspond to the Tersoff and Hamann approximation of Eq. (1), i.e., plots are proportional to current at a constant tip height. Experimental data shown here are in all cases constant current images,

Table 1
Platinum EHT parameters

Orbital	Valence orbital ionization potential (eV)	Slater exponent
5d	−12.59	6.013 (0.6334) 2.696 (0.5513)
6s	−9.077	2.554
6p	−5.475	2.554

where grey-scale level represents tip height, requiring some rescaling of the calculational data for meaningful comparison. Since an order of magnitude change in tunneling current corresponds to approximately 1 Å of tip–sample separation, base ten logarithms of the calculated plots are presented here. Although no specific inclusion of the tip in the calculation is made, the effects of a finite, non-perfect tip on the experimental data are apparent, and this effect has been incorporated by convolving calculated electronic structures with a Gaussian of 1 Å FWHM. A 0.5 Å FWHM tip did not noticeably broaden the images, while a 1.5 Å FWHM tip provided insufficient resolution when compared with experimental images.

4. Results and discussion

4.1. Determination of computational method

In the theory of Tersoff and Hamann, the simplifying assumption of a point tip determines that only electronic states at the Fermi level should contribute to the tunneling images. Such calculations would therefore yield point-density-of-states images. For real tunneling systems with finite-size tips and nonzero tunneling bias, of course, coupling will occur for all electronic states between the Fermi level and that bias. In the case of isolated molecule calculations, the molecular orbitals near the Fermi level are separated by large energy gaps, on the order of eV's, so that only single electronic states can contribute to the images. But, for adsorbed molecules, surface electronic structure involves a continuum metal band structure and subsequently broadened adsorbate molecular states. This continuum structure is not adequately incorporated within calculations involving small metal clusters, such as performed here. To approximate such structure, it is reasonable that images be computed by including structure from states which fall within an appropriate energy window, i.e., broadening must be artificially incorporated. To illustrate these observations, it is instructive to consider a variety of calculations involving single states.

Fig. 3 shows electronic structures for the LUMO calculated for the six simple adsorption geometries given in Fig. 2, as well as the LUMO of the isolated naphthalene molecule. Several effects are apparent from comparing the isolated molecule LUMO with those which directly include the metal substrate. First, there is a clear influence of the metal cluster on the unoccupied state images for each of the adsorbate geometries. The LUMO for the isolated molecule is clearly elongated in the direction of the long physical axis, but the electronic structure has a six-lobed structure. Proximity to the metal cluster does not remove the elongation, but does substantially alter the internal electronic structure features. That the origin of this new internal structure is the metal orbitals is obvious from the differences due to adsorbate position. Although all the molecules in Fig. 3

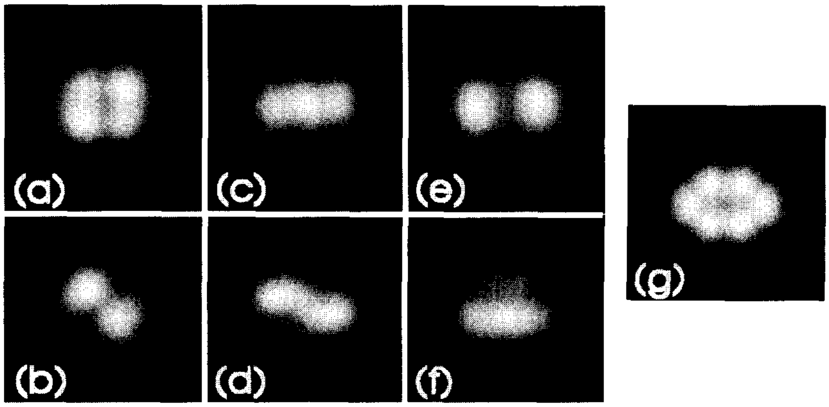

Fig. 3. Grey-scale plots of LUMO's for naphthalene adsorbed on platinum; (a) through (f) correspond to the adsorption geometries shown in Fig. 2. (g) The LUMO for isolated naphthalene.

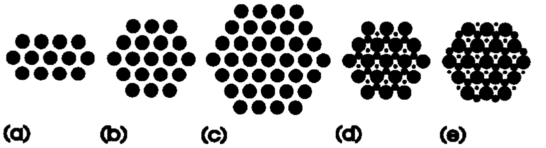

Fig. 4. Schematic diagrams of five platinum clusters used for tests of sensitivity of electronic structures to cluster size and symmetry. Single layer clusters: (a) Pt_{13}, (b) Pt_{19}, (c) Pt_{37}. Triple layer clusters: (d) Pt_{43} and (e) Pt_{55} (smaller dots indicate lower layer atoms).

are positioned horizontally in the center of the plots, the orientation and structure of the apparent molecular electronic structure is not necessarily horizontal or even symmetric about the molecular axes. Comparison of the LUMO plots with the structures in Fig. 2 demonstrates that intensity is not localized over molecular bonds, but rather over underlying metal features. Thus, as in Fig. 3b, when the metal cluster is rotated by 30° with respect to the axis of the molecule, the apparent STM image also rotates.

This influence of the adsorbate site symmetry upon the calculated electronic structure is quite promising because it suggests the ability to assign adsorption sites directly by comparison of experimentally acquired images with model calculations. Such assignments have been made for the adsorption of benzene on graphite [10] and on Pt(111) [11]. It is, however, important to explore the implications of various computational variables other than adsorption site and orientation, such as the size and symmetry of the metal cluster. Fig. 4 displays five platinum clusters utilized to investigate such effects for a given adsorption geometry – naphthalene in the low-energy site of Fig. 2a. The first three clusters are single layer clusters with 13, 19 and 37 atoms, respectively. The Pt_{13} cluster is elongated, in contrast to the six-fold symmetry of the Pt_{19} and Pt_{37} clusters. While the Pt_{13} and Pt_{19} clusters have maximum dimensions comparable to the maximum dimensions of naphthalene, the Pt_{37} cluster is large enough to eliminate potential interactions between the molecule and metal perimeter atoms. The final two clusters incorporate three layers of platinum atoms, to examine the effects of subsurface site symmetry. Fig. 5 displays the corresponding calculated LUMO images. It is immediately apparent that substantial differences in the electronic structures for the same molecular site are introduced by the different metal clusters. This effect can be readily understood by considering the nature of these calculations.

The molecular orbitals for the isolated naphthalene molecule are well-separated and distinct, with an energy gap between the LUMO and HOMO of approximately 3 eV. The energy separations between orbitals for the metal cluster are much smaller, and as the number of atoms in the cluster increases, the overall structure must ultimately approach the metal band structure. For the adsorbed molecule, mixing between molecular and metal orbitals will occur, but as already demonstrated by the sensitivity to adsorption site, the LUMO appears strongly dependent upon the underlying metal orbitals. An easy way to visualize the interaction between molecule and metal orbitals is shown in Fig. 6, where the fraction of each orbital which originates from the molecule is plotted, for twenty orbitals on either side of the Fermi energy, for the five platinum clusters indicated in Fig. 4. As the size of the platinum cluster increases, those orbitals with predominantly molecular character can be seen to separate and move away from the Fermi level. In effect, the LUMO and HOMO may become dominated by metal orbitals, and as more metal orbitals are introduced with smaller energy gaps separating individual orbitals, symmetry requirements may substantially affect the appearance

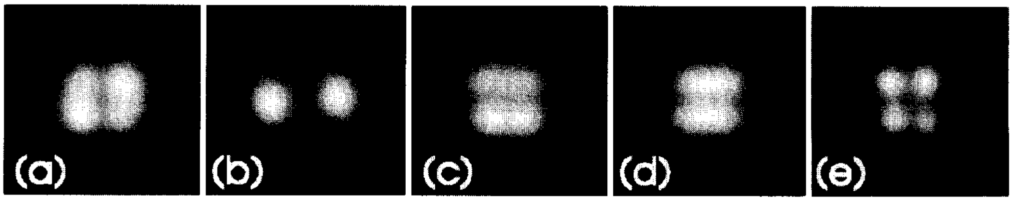

Fig. 5. Grey-scale plots of LUMO's for naphthalene adsorbed in an on-top site, with long axis parallel to the metal near-neighbor direction, for each of the platinum clusters shown in Fig. 4.

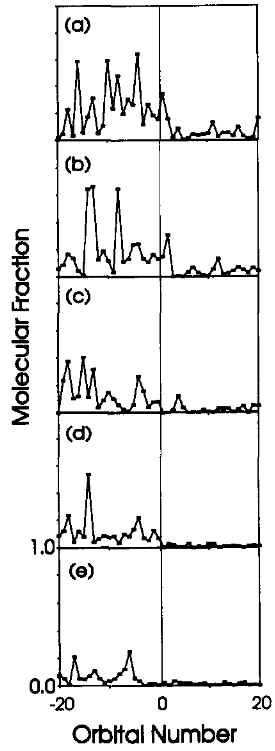

Fig. 6. Plots of normalized molecular contribution to each orbital for the molecule/metal system. Twenty orbitals on each side of the Fermi level (marked by 0) are shown; (a) through (e) correspond to the computations of Fig. 5 for the clusters shown in Fig. 4. As the number of metal atoms increases, those orbitals near E_F become more predominantly metal in character.

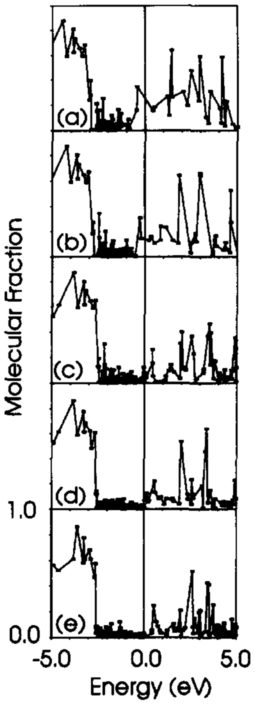

Fig. 7. Normalized molecular contribution to each orbital for the molecule/metal system, plotted as a function of energy, with E_F at 0 eV; (a) through (e) as in Fig. 6. The number of orbitals near the Fermi level obviously increases as the number of platinum atoms in the cluster rises, and molecularly dominated orbitals mix with these metal orbitals and become more diffuse.

of the LUMO or HOMO. In Fig. 7, the fraction originating from the molecule for each orbital is now plotted as a function of *energy*, and it is apparent that while some movement and distribution of molecular density does occur, the overall effect is one of increasing the density of metal states. Thus, as already explained, it is clearly not reasonable to simply plot LUMO or HOMO density for comparison with experimental images.

As mentioned previously, the appropriate method involves summing over a range of orbitals with energies near the tunneling bias. Because the STM images are typically acquired with relatively low tip–sample bias, 0.1–1 eV, an energy window of 0–1 eV provides a qualitatively justifiable range for such sums. More importantly, this value is also a reasonable estimate of the typical broadening of molecular levels induced by interactions with a metal substrate [12]. Plots resulting from summing over all

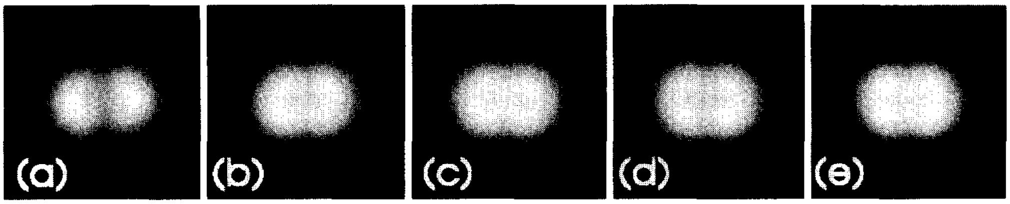

Fig. 8. Grey-scale plots of unoccupied LDOS within 1 eV of the Fermi level, for naphthalene adsorbed in the site shown in Fig. 2a. The five plots correspond to the five different platinum clusters shown in Fig. 4.

unoccupied orbitals within 1 eV of the Fermi level are shown in Fig. 8 for the same five metal clusters examined previously. Hence, when all molecule–metal system electronic levels accessible in the STM experiment are included in the computed images, i.e. when the calculation adequately approximates the continuum nature of the surface system and includes non-zero tunneling bias, there appears to be no strong influence of cluster lateral extent or thickness upon the images. This result implies that the important interactions between the adsorbed molecule and the metal substrate, at least from the point of view of the STM, arise from mixing of states from nearby atoms and from adsorbate site geometry, i.e. interactions with more distant metal surface and subsurface atoms are less significant. Increasing the width of the energy window does not significantly influence either the qualitative internal structure or the resolution of the calculated STM images for the molecules examined here. A broader window may be necessary, however, for adsorption situations where longer range surface interactions are important, where higher STM tunneling energies are used, or in situations where interactions between tip and surface become dominant.

To readdress the question of site sensitivity, summations of unoccupied states within 1 eV of the Fermi level are plotted in Fig. 9 for each of the adsorption geometries shown in Fig. 2. Comparison of these plots with those of Fig. 3 reveals that the broadening has somewhat reduced the striking differences among electronic structures, as might be expected. For the two geometries where naphthalene is rotated by 30° with respect to the metal lattice directions (Figs. 9b and 9d) there is an obvious change in the electronic structures, as compared to the remaining geometries with naphthalene rotated by either 0° or 90°. In the latter adsorption sites, the molecules look quite similar, but with a noticeable bi-lobed structure in the on-top, 0° site. This bi-lobed character is very clearly present in experimental images of naphthalene on Pt(111) and corresponds to the assigned adsorption site. The binding energy curves utilized earlier in the computational procedure (see Fig. 1) to set the molecule–metal separation, are now again useful in differentiating adsorption sites that are energetically favorable as well as appropriately structured electronically.

The computational procedure to be followed is now quite clear. For a given adsorbate system, energy minimization is performed for a variety of adsorption sites and orientations. The low-energy geometry is then utilized to calculate the electronic levels for the combined molecule–metal system. For either occupied or unoccupied state plots, sums of all orbitals within a given energy range, typically 1 eV, are plotted at a selected height above the molecule. Note that in cases where EHT calculated chemisorp-

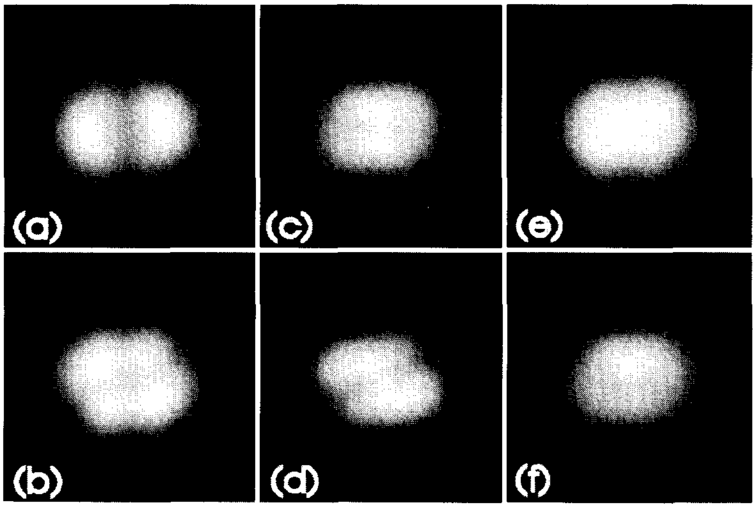

Fig. 9. Unoccupied LDOS for naphthalene adsorbed in the corresponding six geometries shown in Fig. 2.

tion energies for several sites are comparable in energy, it is expedient to compare computed images with experimental images to determine (if possible) the actual adsorption geometry. Of course, if the geometry is known from experiment, energy minimization is unnecessary, but may be otherwise instructive.

4.2. Comparison of computed and experimental images

While this methodology described above has been developed for the case of naphthalene adsorbed on Pt(111), comparisons with experimental data will encompass related systems as well, in order to ascertain the generality of this technique. The other molecular systems which have been experimentally imaged [3] include azulene, 1-, 2- and 6-methylazulene (1-MA, 2-MA, 6-MA), 4,8-dimethylazulene (DMA) and 4,6,8-trimethylazulene (TMA). The molecular structures and their sizes relative to the Pt_{13} cluster are shown in Fig. 10 making obvious that while this cluster may be reasonable for the smaller species, a larger cluster such as Pt_{19} or Pt_{37} might be required for more accurate calculations for larger molecules such as DMA or TMA. Adsorption site geometries are derived from binding energy minimizations, and are in accord with experimental assignments [3].

Experimental data for a representative selection of the investigated molecules are shown in Fig. 11 along with predictions from the calculations for both isolated molecules and the molecule/metal systems described here. The images produced when the effects of the metal cluster are included are much superior to those for the molecule alone in several respects. For example, two experimental images are shown for naphthalene on Pt(111) – the typical "low-resolution" image (Fig. 11b) and a more difficult to acquire "high-resolution" image (Fig. 11a). The former exhibits the elongated, bi-lobed structure previously described, while the latter clearly resolves the double-ring structure of this molecule. While the high-resolution type image is relatively infrequently acquired, presumably because of difficulty in attaining the appropriate tunneling tip structure or composition, such images are typically acquired at lower tip–sample separation. Plots of the calculated adsorbate and isolated molecule structures are shown at two different heights above the plane of the molecular ring system. At an elevation of 2 Å, the adsorbate LDOS plot (Fig. 11d) reproduces well the bi-lobed

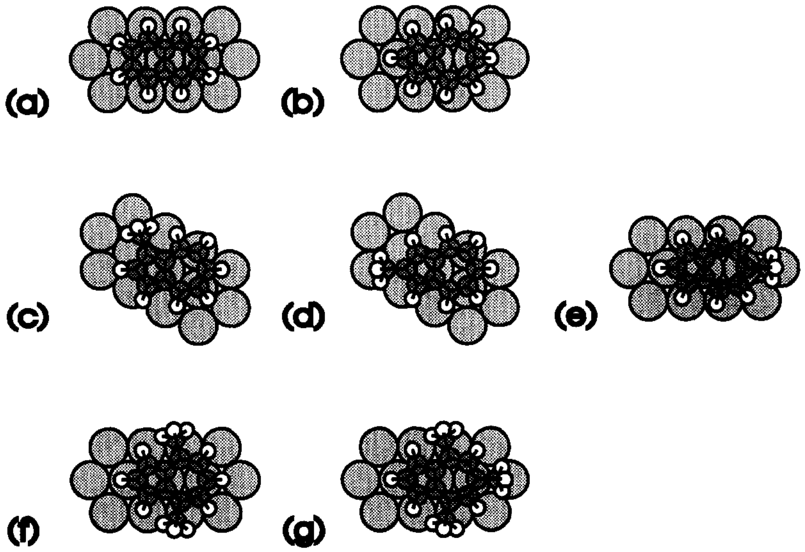

Fig. 10. Comparisons of molecular dimensions with those of the Pt_{13} cluster: (a) naphthalene, (b) azulene, (c) 1-methylazulene (1-MA), (d) 2-methylazulene (2-MA), (e) 6-methylazulene (6-MA), (f) 4,6-dimethylazulene (DMA) and (g) 4,6,8-trimethylazulene (TMA). The displayed molecular orientation with respect to the metal lattice, as assigned from experiment, is used in subsequent calculations.

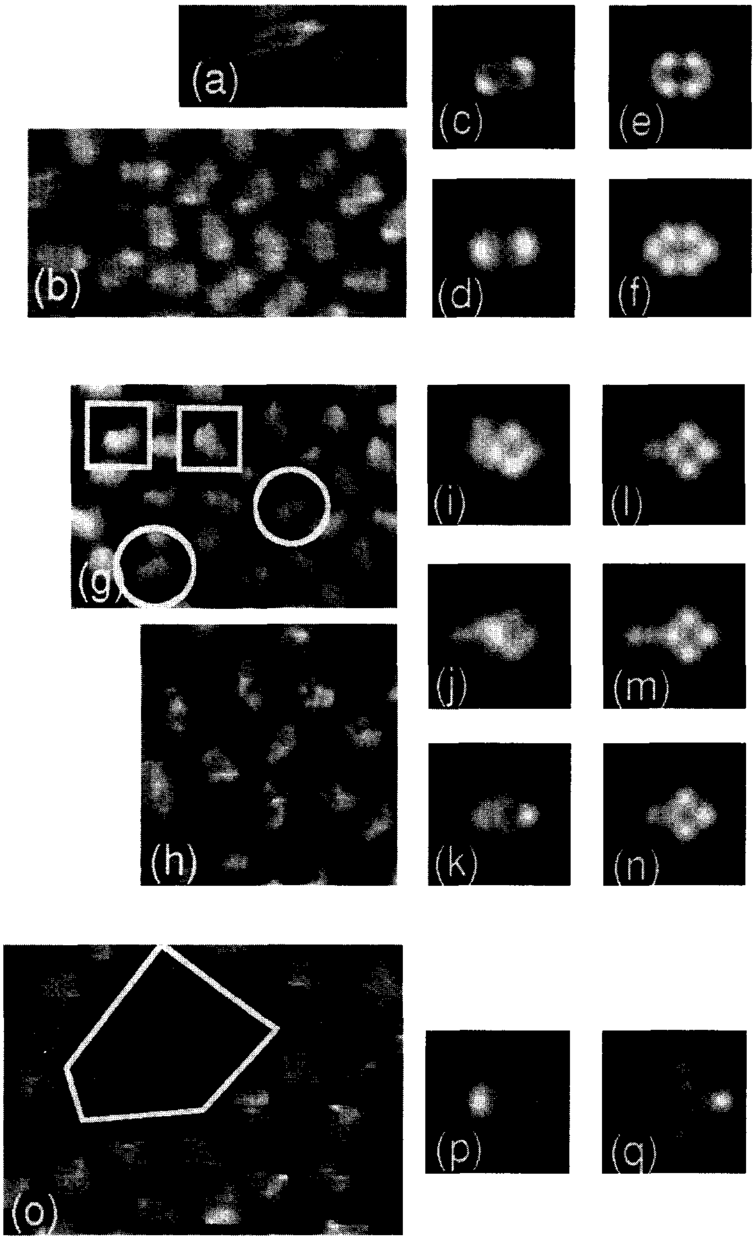

Fig. 11. (a) Typical high-resolution and (b) low-resolution experimental images of naphthalene. Unoccupied LDOS for naphthalene at (c) 0.5 Å and (d) 2.0 Å above the molecular ring plane. Isolated molecule LUMO at (e) 0.5 Å and (f) 2.0 Å above the molecular plane. (g) Low-resolution experimental image of coadsorbed 1-MA (e.g., squares) and 2-MA (e.g., circles). (h) High-resolution experimental image of 6-MA. Unoccupied LDOS for (i) 1-MA (2.0 Å elevation), (j) 2-MA (2.0 Å) and (k) 6-MA (0.5 Å). Isolated molecule LUMO at same elevations for (l) 1-MA, (m) 2-MA and (n) 6-MA. (o) Experimental images of coadsorbed TMA and naphthalene (inside marked area). (p) LDOS and (q) isolated molecule LUMO at 2.0 Å elevation.

character of the low-resolution experimental image, while the six-lobed structure of the isolated molecule LUMO (Fig. 11f) does not agree very well. When the elevation in the calculations is reduced to 0.5 Å, correspondence between the isolated molecule (Fig. 11e) and the high resolution experimental images is even poorer, with the calculation predicting a node along the bridge bond between the rings while the data demonstrate clear intensity in that position. However, the adsorbate LDOS (Fig. 11c) predicts the correct double-ring structure quite clearly. This result indicates that resolution effects, in the case of a point tip, can be reproduced in the calculation by investigating the two-dimensional electronic structure as a function of elevation.

When a single methyl group is substituted at various positions on the azulene ring system, the excellence of the fit with the adsorbate LDOS is even more pronounced. For substitutions at the 1- or 6-positions, the isolated molecule LUMO's do not exhibit significant intensity contributions at the positions of the methyl groups (Figs. 11l and 11n), implying that these two isomers could not be distinguished by STM measurements. These two molecules are very different in the STM data, in disagreement with the isolated molecule calculation, but the experimental images agree very well with the LDOS plots for the adsorbed molecules (Figs. 11i and 11k). The methyl group intensity appears in the correct position for all three isomers, and the internal ring structure and slightly higher intensity over the methyl group noted in the high-resolution images of 6-MA are again reproduced by LDOS plots at lower elevation (Fig. 11k).

In the case of TMA, interpretation of the STM data would be incorrect in one notable respect if comparison was limited to the isolated molecule LUMO calculation. This molecule displays a four-leaf-clover structure, with one lobe typically of higher intensity (Fig. 11o). Simple symmetry and electron density arguments might lead to assignment of the brighter lobe to the 5-carbon ring, but the isolated molecule LUMO actually shows that the higher intensity is localized over the methyl group at the 6-position (Fig. 11q). This is rather curious, since the same bright lobe is present in images of DMA [3], where no methyl group exists at that position. On the other hand, including the metal substrate in the computation results in intensity on the 5-carbon ring as speculated (Fig. 11p), yielding consistency for the two different adsorbates.

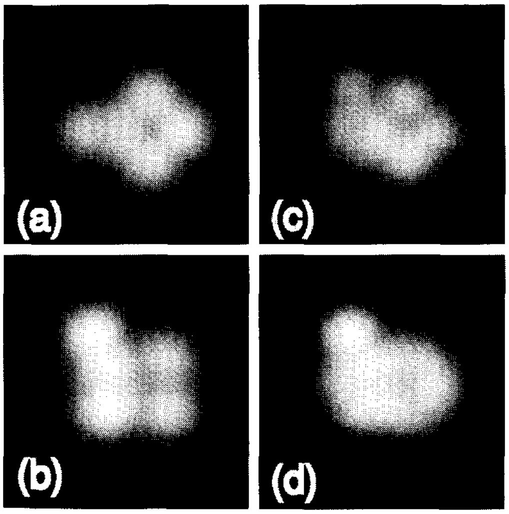

Fig. 12. Calculations for 1-MA on both sides of the Fermi level. Isolated molecule LUMO (a) and HOMO (b). Adsorbate LDOS, unoccupied (c) and occupied (d).

To understand the origin of the discrepancy between the experimental images and those from the isolated molecule calculations requires consideration of the orbitals on either side of the Fermi level. Fig. 12 shows both the LUMO and HOMO for isolated 1-MA, along with unoccupied and occupied LDOS images as calculated by the procedure described above. It is immediately apparent that the HOMO and LUMO differ substantially, not only in the electronic structure of the ring system, but also in that the methyl group appears strongly in the HOMO, but not significantly in the LUMO. In contrast, the unoccupied and occupied LDOS plots are quite similar, as are unoccupied and occupied states experimental images. The interaction of the molecular states with those of the metal substrate effectively causes mixing of both LUMO and HOMO character with the underlying metal electronic structure, so that the composite structures are comparable in detail on either side of the Fermi level. Interestingly, as depicted in Fig. 7, the contribution of the molecular levels to the adsorbate electronic structure appears to be qualitatively similar but quantitatively less for occupied states as compared to unoccupied states.

This observation is in agreement with experiments on these adsorbate systems, where changing the sign of the tunneling bias does not typically reveal different molecular structures, but occupied states imaging can seem technically more difficult to perform.

4.3. Extension to other systems

It is interesting to speculate upon the suitability of this computational technique for providing accurate LDOS images for other molecules and/or substrates. To test general applicability, images for three other systems of interest are presented here. The first example is the case of graphite, a very commonly used STM substrate, which exhibits the interesting feature that typical STM images resolve only half of the surface atoms [13] due to electronic structure effects. Previous studies of benzene and carbon monoxide coadsorbed on Rh(111) provide another, more involved, examination of the capabilities of the calculational method for yet a different substrate, and two different molecules adsorbed simultaneously. Finally, a prediction of electronic structure for a system not yet studied by STM is made for the system of fluorobenzene on Pt(111).

The structure and LDOS plots of a graphite cluster are shown in Fig. 13. Two layers of hexagonally bonded carbon are included in this calculation. Previous theoretical studies [14] of this surface have attributed lower intensity over half of the surface atoms to an electronic effect arising from layer interactions between carbon atoms. Those surface carbon atoms which have neighbors directly below them in the second layer have been assigned to the lesser intensity locations on the graphite lattice, so that the overall images appear to resolve only every other atom. This interpretation is consistent with the LDOS image calculated here. The net result is an image which appears to have bright features arranged with hexagonally close-packed symmetry, while less intense features are characteristic of those surface atoms with neighbors in the second layer, as previously observed experimentally [13]. A noticeable boundary effect is present, where those bright atoms on the perimeter of the cluster are even brighter than the analogous carbons nearer the lateral center of the cluster, but the effect is nevertheless present away from the cluster edges.

Benzene and carbon monoxide coadsorbed on Rh(111) at appropriate coverage from a (3 × 3) structure with two carbon monoxide molecules and one benzene molecule per unit cell [15]. In STM studies of this system [16], several electronic effects were invoked in interpretations of the images. First, the three-lobed appearance of the benzene molecules rather than the expected six-fold symmetry was attributed to interactions with the underlying three-fold hollow Rh site. Analysis of the binding site symme-

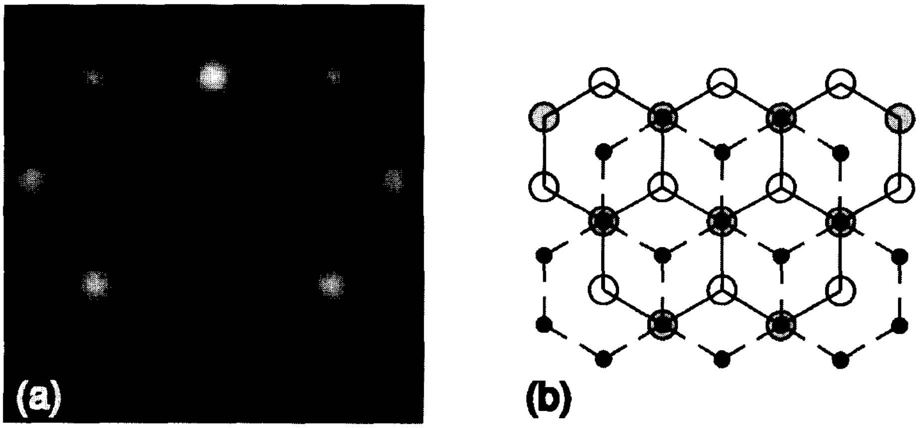

Fig. 13. Calculated unoccupied LDOS (a) for a two layer graphite system, schematically shown in (b). Large open circles represent the top layer carbon atoms, while small filled circles represent the second-layer carbon atoms. Lower intensity is observed for those top layer atoms which overlay atoms in the second layer (superimposed small and large circles).

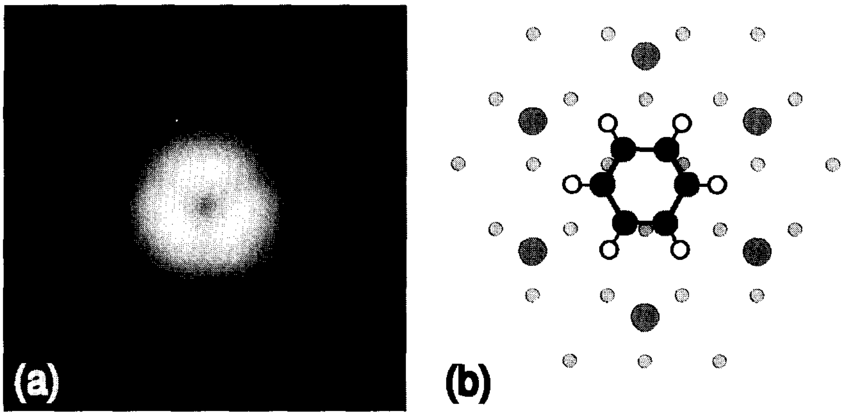

Fig. 14. (a) Calculated unoccupied LDOS for benzene and CO coadsorbed on a Rh(111) cluster. (b) Schematic of system used for the calculations, where the small grey circles represent the Rh atoms, the large grey circles show the positions of the CO molecules and the white and black connected circles depict the benzene molecule.

try allowed assignment of the observed nodes at positions over underlying metal atoms. Despite similar physical heights of the carbon monoxide and benzene molecules, the observed STM height at the CO positions was only ~ 10% of that for the benzene, also ascribed to an electronic effect whereby fewer electronic states of the CO molecule were available under the tunneling conditions employed for the images. Utilizing the atomic positions determined from detailed LEED investigations [15], and published rhodium EHT parameters [17], the calculated LDOS image shown in Fig. 14 reproduces all of these observed effects. In the calculations, neither the presence of the CO molecules nor Kekule distortion of the molecule by binding to the rhodium lattice, yielding alternating shortened and lengthened C–C bonds, is necessary to produce the three-lobed apparent structure of the benzene molecules, al-

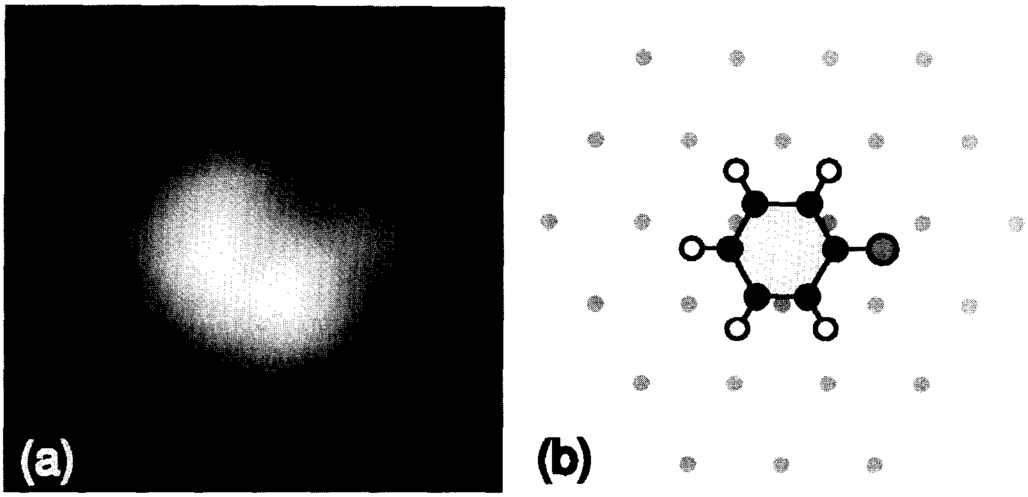

Fig. 15. (a) Calculated unoccupied LDOS for fluorobenzene adsorbed on a Pt(111) cluster, in the arrangement shown in (b) where the fluorine substituted onto the phenyl ring is represented by the large grey-filled circle.

though the latter effect does slightly enhance the node structure. In the STM study, only three of the carbon monoxide molecules were readily resolved, and it was not clear whether the remaining three CO's were indeed different due to their positions in the unit cell or if some asymmetry in the tunneling tip obscured those molecules. In the calculated images, no obvious differences among the six carbon monoxide molecules are evident.

The effect of halogen substitution upon the electronic structure as probed by STM is an interesting question. One possible expectation is that the high electron density localized around, for example, a fluorine atom might make such features more intense and notable in STM images. It is somewhat surprising that this is not the situation predicted by the LDOS calculation. Fig. 15 reveals that the apparent LDOS near the fluorine position for the case of fluorobenzene adsorbed on Pt(111) is reduced compared to the phenyl ring, while intensity within the ring system, directly over the nearest underlying Pt atom, is quenched. This observation thus provides an interesting test of this computational method, since studies of this system have been proposed but no known experimental results are available for comparison. The results of this calculation also imply that simple analysis of localized electron density in isolated molecules is not necessarily a valid basis for assigning experimentally observed features in STM data.

5. Conclusions

A reasonable computational methodology has been developed for calculating STM images of adsorbed molecules. For adsorbate systems with unknown adsorbate geometry, chemisorption energy minimization using EHT methods is used to determine the low energy adsorption site(s) and orientation(s) for a molecule plus metal cluster. The actual or tentative geometry is then used to calculate extended Hückel orbitals for the molecule/metal system. Energy integration of contributions from all orbitals at a selected elevation then yields plots of occupied or unoccupied local density of states to be compared with STM data. Images generated in this manner exhibit excellent agreement with experimentally acquired STM images for a variety of molecular adsorbate systems on Pt(111), as well as for a graphite cluster and the benzene and carbon monoxide on Rh(111) coadsorbate system. This method has been used to predict the expected STM image for the case of fluorobenzene adsorbed on Pt(111), for comparison to future experiments.

Several general comments can be made about the insights gained from these calculations. First, inclusion of the metal substrate interaction with the adsorbate molecule is necessary for correct interpretation of STM data in systems where significant mixing of molecular and metallic states occurs. Second, there appears to be sufficient sensitivity of the computed images to adsorbate binding site and orientation to permit assignment of these geometric parameters from comparisons of experimental and calculated images. This observation is supported by recent experimental data [18] and more involved electron scattering calculations [11]. Third, although resolution is critically dependent upon experimental tip effects, there is good correlation between observed internal molecular structure and effective tip–sample separation. Finally, tip bias effects also are well reproduced by this calculation, i.e. mixing of spatially very different occupied and unoccupied isolated molecule states via interaction with the metal substrate can lead to close similarity between adsorbate occupied and unoccupied images.

Obvious extensions of this computational method are possible. For example, it is likely to be necessary to impose a more involved energy minimization routine for adsorbate systems where molecular geometries are significantly modified by strong interactions with the metal surface, or where EHT methods otherwise do not give good qualitative trends. As discussed in the methods section, images shown here are effectively constant height plots, although all experimental data shown were constant current images. It is of course reasonable to modify the present procedure to calculate heights as a function of constant electron or hole density, rather than utilizing the oversimplified logarithmic approximation employed here. Explicit incorporation of tunneling between the sample and a tip with specified structure and electronic states, is another possible modification which might allow investigation of the effects of particular tip geometries upon the molecular images.

Comparison of this computational procedure with those developed by other groups is also of interest. For example, electron scattering calculations have been performed for benzene on Rh(111) [19], where the complete substrate–molecule–tip system is included. That study did not, however, incorporate the coadsorbed carbon monoxide molecules, so that no conclusions can be drawn regarding relative intensities. That investigation did infer that interference effects between the tip and sample were important to derive the appropriate symmetry in the computed image, an effect which is clearly not present, and which appears unnecessary, in the procedure used here. Another interesting feature of the presumably more accurate scattering calculation is that the lateral extent of the images appears to exceed that of the molecule by approximately 40% [20]. In contrast, the adsorbate LDOS images shown here have lateral extent comparable to the physical sizes of the molecular adsorbates. Given that the computational procedure described here is very simple and fast when compared to the more involved and computationally intensive electron scattering calculations, the good agreement between experiment and theory is even more impressive.

It is hoped that the simple computational method developed herein will prove useful in predicting STM images of molecular adsorbates. In particular, the ability to distinguish among very similar molecules, for example isomers, has significant implications for future studies of molecular surface reactions. A simple, efficient calculational method would serve as a guide to determining the prospects of differentiating among reactants, intermediates and products by STM prior to beginning the much more intricate experimental studies.

Acknowledgements

The authors would like to acknowledge helpful discussions with Ch. Wöll, P. Sautet and C. Joachim.

References

[1] P.H. Lippel, R.J. Wilson, M.D. Miller and Ch. Wöll, Phys. Rev. Lett. 62 (1991) 171.
[2] D.P.E. Smith, J.K.H. Hörber, G. Binnig and H. Nijoh, Nature (London) 344 (1990) 641.
[3] V.M. Hallmark, S. Chiang, K.-P. Meinhardt and K. Hafner, Phys. Rev. Lett. 70 (1993) 3740.
[4] J. Tersoff and D.R. Hamann, Phys. Rev. Lett. 50 (1983) 1998.
[5] W.H. Flygare, Molecular Structure and Dynamics (Prentice-Hall, Englewood Cliffs, NJ, 1978) p. 367.
[6] A. Gavezotti, E. Ortoleva and M. Simonetta, Chem. Phys. Lett. 98 (1983) 536.
[7] R. Hoffman, Rev. Mod. Phys. 60 (1988) 601.
[8] V.M. Hallmark, S. Chiang, J.K. Brown and Ch. Wöll, Phys. Rev. Lett. 66 (1991) 48.
[9] A. Gavezotti and M. Simonetta, Surf. Sci. 9 (1980) 453.
[10] A.J. Fisher and P.E. Blochl, Phys. Rev. Lett. 70 (1993) 3253.
[11] P. Sautet and M.L. Bocquet, Surf. Sci. 304 (1994) L445.
[12] P. Norlander and N.D. Lang, Phys. Rev. B 44 (1991) 13681.
[13] G. Binnig, H. Fuchs, Ch. Gerber, H. Rohrer, E. Stoll and E. Tosatti, Europhys. Lett. 1 (1986) 31.
[14] I.P. Batra, N. Garcia, H. Rohrer, H. Salemink, E. Stoll and S. Ciraci, Surf. Sci. 181 (1987) 126.
[15] R.F. Lin, G.S. Blackman, M.A. Van Hove and G.A. Somorjai, Acta Cryst. B 43 (1987) 368.
[16] H. Ohtani, R.J. Wilson, S. Chiang and C.M. Mate, Phys. Rev. Lett. 60 (1988) 2398.
[17] A. Gavezzotti, E. Ortoleva and M. Simonetta, J. Chem. Soc. Faraday Trans. I, 78 (1982) 425.
[18] P.S. Weiss and D.M. Eigler, Phys. Rev. Lett. 71 (1993) 3139.
[19] P. Sautet and C. Joachim, Chem. Phys. Lett. 185 (1991) 23; Surf. Sci. 271 (1992) 387.
[20] C. Joachim, private communication.